

# Simple Cues Lead to a Strong Multi-Object Tracker

Jenny Seidenschwarz, Guillem Brasó, Ismail Elezi, and Laura Leal-Taixé

Technical University of Munich

**Abstract.** For a long time, the most common paradigm in Multi-Object Tracking was tracking-by-detection (TbD), where objects are first detected and then associated over video frames. For association, most models resource to motion and appearance cues. While still relying on these cues, recent approaches based on, *e.g.*, attention have shown an ever-increasing need for training data and overall complex frameworks. We claim that 1) strong cues can be obtained from little amounts of training data if some key design choices are applied, 2) given these strong cues, standard hungarian matching-based association is enough to obtain impressive results. Our main insight is to identify key components that allow a standard reidentification network to excel at appearance-based tracking. We extensively analyse its failure cases, and show that a combination of our appearance features with a simple motion model leads to strong tracking results. Our model achieves state-of-the-art performance on MOT17 and MOT20 datasets outperforming previous state-of-the-art trackers by up to 5.4*pp* in IDF1 and 4.4*pp* in HOTA. We will release the code and models after the paper’s acceptance.

**Keywords:** Multi-Object Tracking, Person Re-Identification

## 1 Introduction

Multi-Object Tracking (MOT) aims at finding the trajectories of all moving objects in a video. For a long time, the dominant paradigm in the field was tracking-by-detection, which divides tracking into two steps: (i) frame-wise object detection, (ii) data association to link the detections and form trajectories. One of the simplest forms of data association for online trackers is frame-by-frame matching using the Hungarian algorithm [27]. Matching is then driven by cues such as appearance, *e.g.*, re-identification (reID) features [36,21,44,11,56,58,76] or motion cues [75,46,4,65,41].

Even new learning-based trackers still rely on motion priors [4,52,63,80] or appearance cues, which may include external reid models [4,63]. Recent trackers based on Transformers [54,37,71] promise to learn all necessary cues from data through self- and cross-attention between frames and tracked objects. While powerful, these methods rely more and more on large amounts of training data, *e.g.*, pre-training on the detection dataset CrowdHuman [50] has become a necessity to obtain state-of-the-art results.

We argue that if the appearance and motion cues are strong, we do not need a complex tracker, and a simple frame-by-frame tracking-by-detection will suffice. We therefore propose to revisit the roles of the appearance and motion cues for MOT. Our first observation is that simply using state-of-the-art re-identification (reID) networks for appearance matching is not enough for the real scenarios of MOT. In Figure 1, we visualize the performance of several state-of-the-art reID approaches on Market-1501 dataset [78] (x-axis), as well as the models performance when used in a simple matching-based tracker (y-axis). It shows that the reID performance does not necessarily translate to MOT performance.

We identify two problems causing the weak performance of reID models on MOT: (i) reID models need to account for the different challenges expected at different time horizons, *i.e.*, while in nearby frames appearance of objects will vary minimally, in longer time gaps more severe changes are expected, and (ii) reID performance tends to be inconsistent across MOT sequences because of their varying image statistics, which in turn differ from the relatively stable conditions of their reID training dataset. We propose two simple but key design choices to overcome the aforementioned problems, *i.e.*, different policies for active and inactive tracks, and on-the-fly domain adaptation.

We then do an extensive analysis under different conditions of visibility, occlusion time, and camera movement, to determine in which situations reID is not enough and we are in need of a motion model. With a simple combination of our reID and a linear motion model, we obtain a tracking-by-detection tracker without any bells and whistles that significantly outperforms state-of-the-art. Most notably, our reID model is *never trained on any tracking dataset*, showing good generalization.

In summary, we make the following contributions:

- We provide key design choices that significantly boost the performance of reID models for the MOT task.
- We extensively analyze in which cases appearance and motion have the potential to increase performance with respect to current trackers.
- We obtain state-of-the-art results on several benchmarks with a simple tracking-by-detection online tracker.

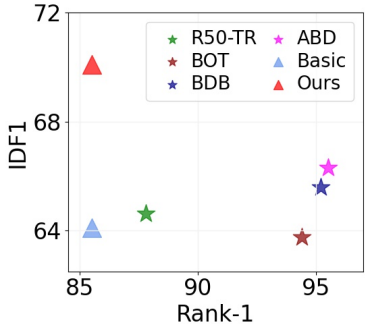


Fig. 1: IDF1/Rank-1 of different state-of-the-art re-ID approaches. R50-TR [79], BOT [36], BDB [15], ABD [10]. *Basic* is our baseline, *Ours* is our appearance model.

## 2 Related Work

In the last years, the TbD paradigm has commonly been used in MOT [4,65,61,75,57,39,40,8,22]. Pedestrians are first detected using object detectors [46,45,66]. Then, detections are associated across frames to form trajectories corresponding to a certain identity utilizing motion, location, appearance cues or a combination of them. The association step can either be solved frame-by-frame for online applications or track-wise over the sequence in an offline manner.

**Graph-Based Approaches.** One common formalism is to perform data association following the TbD paradigm viewing each detection as a node in a graph with edges linking several nodes over the temporal domain to form trajectories. Determining which nodes are connected can then be solved using maximum flow [3] or minimum cost approaches [23,43,73] by, *e.g.*, taking motion models into account [29]. Recent advances combined track-wise graph-based models with neural networks [8]. The aforementioned approaches may work well, but are rather complex. We rethink those recent advances and show that we can obtain strong TbD trackers by combining a common appearance model enhanced with two design choices trained solely on a commonly used person re-identification (ReID) dataset with an linear motion model.

**Motion-Based Association.** Different from the graph-based approaches, many TbD approaches perform frame-by-frame association directly using motion and location cues from detections and existing trajectories [5,6,80,41,39]. For short term preservation, those trackers exploit that given two nearby frames object displacements tend to be small. This allows them to utilize spatial proximity for matching by exploiting, *e.g.*, Kalman filters [5]. Taking this idea further, approaches following the tracking-by-regression paradigm utilize object detectors [4,80] to regress bounding box positions. Recent advances introduced Transformer-based approaches [37,54,71] that perform tracking following the tracking-by-attention paradigm. Using sophisticated motion models, those approaches reach outstanding performance with respect to short-term associations in most scenarios. However, especially the Transformer-based approaches require large amounts of training data. Contrary to all those approaches, in this work we show that a simple linear motion model suffices to model short-term associations in most scenarios. In scenes with moving camera or scenarios requiring non-trivial long-term associations, *e.g.*, scenarios with many occlusions, purely motion-based trackers struggle which calls for a combination with appearance based cues.

**Appearance-Based Association.** To achieve better performance in long-term association scenarios, numerous approaches use additional appearance-based re-identification networks that encode appearance cues to re-identify persons after occlusions [70,4,8,26,62,28,48,51]. Further exploring this direction, a recent work [40] proposed to train a detection network solely utilizing embedding information during the training process. Enhancing MOT towards real-time, several works proposed to jointly compute detections and embeddings in a multi-task setting [65,19,61,34,75]. Some of them introduce more balanced training schemes [19,65] to better leverage the synergies between both cues. While promising, approaches

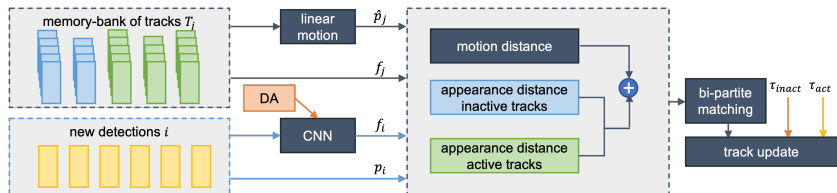


Fig. 2: Overview over our approach where DA represents the domain adaptation. The memory bank contains all **inactive** and **active** trajectories but we process both differently. Each tracklet consists of its feature vector and bounding box positions. We utilize the sum of motion and appearance cues for bipartite matching as well as different thresholds for active and inactive trajectories.

using appearance additionally to motion cues require rather complex association schemes with several steps. Also, complex and highly differing training schedules using ever increasing amounts of data or differing inference strategies make it hard to draw conclusions about what really is driving the progress in the field. In contrast, our approach does not rely on complex procedures but combines light-weight motion and spiced-up appearance cues in a simple yet strong TbD tracker that only requires little training data.

**Person Re-Identification.** In contrast to the tracking domain, the goal of person ReID is to retrieve person bounding boxes from a large gallery that show the same person as a given query image based on appearance cues. However, state-of-the-art ReID models tend to significantly drop in performance when evaluated on out-of-domain samples, *i.e.*, samples coming from other datasets [12,77,81]. This mostly is caused by datasets statistics collected by the batch normalization (BN) layers during training. As during application, person ReID models are applied to different cameras, several approaches on cross-dataset evaluation emerged that transfer the knowledge from given source to given target domains [12,77,81]. Inspired by these works in the field of person ReID, we enhance our appearance model to be better suited for MOT using a simple on-the-fly domain adaptation approach. This directly adapts the models learned training dataset statistics (source domain) to the sequences (target domains).

### 3 Methodology

Our approach represents a simple yet strong online tracker. We start by giving the general pipeline of our method (see Sec. 3.1) and then build our strong appearance model (see Sec. 3.2).

#### 3.1 A simple tracking-by-detection tracker

Visualized in Figure 2, we follow the commonly used tracking-by-detection paradigm, which means our tracker takes as input a set of detections  $\mathcal{O} = \{o_1, \dots, o_M\}$ , each represented by  $o_i = (f_i, p_i)$ .  $f_i$  are appearance feature vectors

generated from the raw detection pixels using a Convolutional Neural Network (CNN) and  $p_i$  is the bounding box position in image coordinates. A trajectory or track is defined as a set of time-ordered detections  $T_j = \{o_{j_1}, \dots, o_{j_{N_j}}\}$  where  $N_j$  is the number of detections in trajectory  $j$ . We store *all* existing trajectories in our memory-bank (see Figure 2). Moreover, each trajectory has a corresponding predicted position  $\hat{p}_j^t$  at time step  $t$ , produced by our linear motion model. During the tracking process detections are assigned to trajectories. If no new detection is added to a trajectory at a given frame, we set its status to **inactive** whereas it remains **active** otherwise. The goal is to find the trajectories  $\mathcal{T} = \{T_1, \dots, T_M\}$  that best match the detections to the underlying ground truth trajectories.

Towards that end, we associate existing detections over consecutive frames utilizing bipartite matching via the Hungarian algorithm as commonly done [75,61,32,5]. The assignment is driven by a cost matrix that compares new detections with the tracks already obtained in previous frames. To populate the cost matrix, we use appearance features, motion cues, or both. Our final tracker utilizes a simple sum of both. To restrict assignments to only contain sufficiently similar detection-trajectory pairs  $(i, j)$ , we filter the matchings using matching thresholds  $\tau_i$ .

### 3.2 Strong appearance model for MOT

Our appearance model is based on ResNet50 [20] with one additional fully-connected layer at the end for downsampling, trained on a common person reID dataset [78] using label smoothed cross-entropy loss. It is important to note that *we do not train any part of our reID model on any MOT dataset*. As we will show in experiments, this basic reID model does not perform well on the MOT task. We therefore propose two design choices to make our appearance model stronger: (i) we handle active and inactive tracks differently during embedding distance computation; (ii) we add on-the-fly domain adaption to our model.

**Different handling of active and inactive tracks.** We consider a track to be inactive when the method can no longer track it in the current frame. All other tracks are considered active. Typically trackers only keep inactive tracks for several frames in their memory-bank [4,52,75,46,32], which means they will only be able to re-identify the target after a short occlusion. With our strong appearance model, we are able to keep *all* inactive tracks in the memory bank for association, hence, we are theoretically able to recover the identity after an occlusion of arbitrary length.

While the appearance embeddings of one identity barely vary between two consecutive frames, the embeddings of the same identity before and after occlusion can show larger distances due to, *e.g.*, partial occlusion or varying poses. This pattern can be observed in Fig 3(a), where we plot the histograms of distances between new detections and **active** or **inactive** tracks. In dark colors, we show the distance to a new detection of the same identity (positive match), while in light color we show the distance to a new detection of a different identity (negative match). As we can see, the two dark coloured histograms vary significantly,

suggesting that a different treatment of active and inactive tracks is necessary. Furthermore, we can see the overlap between both negative matches and positive matches for inactive tracks, showing the inherent difficulty of matching an object after a long occlusion.

For active tracks, we leverage the appearance feature vector of the detection assigned to track  $j$  at frame  $t - 1$   $f_j^{t-1}$  for the embedding distance computation to detection  $i$  at frame  $t$ :

$$d_{i,j} = d(f_i, f_j^{t-1}) \quad (1)$$

For the inactive tracks we compute the distance between the appearance feature vectors of all  $N_k$  detections in the inactive track  $k$  and the new detection  $i$  and utilize the mean of those distances as a *proxy distance*:

$$d_{i,k} = \frac{1}{N_k} \sum_{n=1}^{N_k} d(f_i, f_k^n) \quad (2)$$

This leads to a more robust estimate of the true underlying distance between a detection and an inactive track. Hence, in contrast to when using a single feature vector of the inactive track (see Fig 3(a)) utilizing the proxy distance computation leads to better separated histograms (see Fig 3(b)).

Moreover, the different histograms of active and inactive trajectories call for different handling during the bipartite matching. To be specific, during the bipartite matching, thresholds typically determine up to which cost a matching should be allowed. Looking at Fig 3(b), different thresholds  $\tau_i$  optimally divide the histograms of distances from **active** and **inactive** trajectories to detections of the same (dark colors) and different (pale colors) identities. Therefore, we utilize *different matching thresholds*  $\tau_{act}$  and  $\tau_{inact}$  for active and inactive trajectories but we keep one single matching.

**On-the-fly Domain Adaptation.** As introduced in Section 2, recent developments in the field of person ReID propose to apply domain adaptation techniques as the source dataset statistics may not match the target ones [12,77,81].

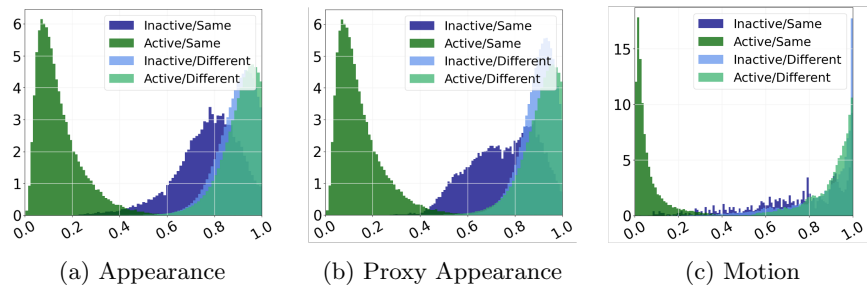


Fig 3: Distance histograms when utilizing (a) the appearance features of the last detection for active and inactive trajectories, (b) the appearance features of the last detection for active and the proxy distance for appearance features of inactive trajectories, (d) the motion distance using IoU measure for active and inactive trajectories.

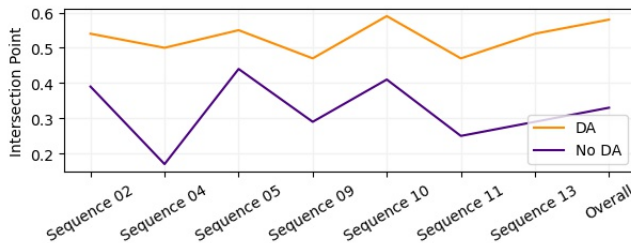


Fig. 4: Visualization of the intersection points between distance histograms from detections to active tracks of the same and different identities when using domain adaptation (DA) compared to when not using it.

For MOT this is an even bigger problem, since each sequence follows different statistics and represents a new target domain. We therefore propose to apply an on-the-fly domain adaptation in order to be able to capitalize on the good performance of reID models when applied to varied MOT sequences. Towards this end, at the different batchnorm layers of the architecture, we utilize the mean and variance of the features of the current batch, which corresponds to the detections in one frame. This approximates the statistics of the sequences reasonably well as all images of one sequence have highly similar underlying distributions, leading to more similar distance histograms across tracking sequences.

Given two distributions  $f_1(x)$  and  $f_2(x)$  they intersect at the intersection point  $x_{1,2}$  where  $f_1(x_{1,2}) = f_2(x_{1,2})$ . Instead of distributions, we only can access histograms of distances. Hence, we utilize an approximation to determine intersection points. For the exact determination please refer to supplementary material. Similar intersection points  $x_{s,d}^{act}$  between histograms of distances from detections to active tracks of same and different identities  $f_{act,s}$  and  $f_{act,d}$  across sequences allow to choose a well suited threshold  $\tau_{act}$ . The same holds for the inactive tracks histograms  $f_{inact,s}$  and  $f_{inact,d}$ , and their corresponding threshold  $\tau_{inact}$ . While the  $x_{s,d}^{inact}$  varies little with and without the on-the-fly domain adaptation,  $x_{s,d}^{act}$  varies significantly less across tracking sequences when using our on-the-fly domain adaptation compared to when not using it (see Figure 4). This allows to find thresholds  $\tau_i$  that are well suited for all tracking sequences and directly affects the parameter choices of our appearance model.

Applying those design choices to our appearance model, makes it more robust towards occlusions as well as better suited for the application in different sequences.

## 4 Experiments

In this section, we first give implementation (Section 4.1) and dataset details (Section 4.2). We then ablate our approach with respect to the appearance design choices (Section 4.3). Afterwards, we analyse the strengths of ReID and motion and ablate the performance of single cues (Section 4.4) to show the potential of our approach (Section 4.5). Finally, we demonstrate that our model

achieves state-of-the-art performance on public (Section 4.6) and private detections (Section 4.7) on two public datasets.

#### 4.1 Implementation Details

Our appearance model follows common practice [4,8,14], with a ResNet50 [20] model with one additional fully-connected layer at the end to downsample the feature vectors. We train our model on the Market-1501 dataset [78] using cross-entropy loss for 70 epochs, with an initial learning rate of 0.0001, and decay the learning rate by 10 after 30 and 50 epochs. For optimization, we utilize the RAdam optimizer [31]. Moreover, we add a BN layer before the final classification layer during training and utilize class balanced sampling as in [36]. We resize the input images to  $384 \times 128$  and apply random cropping as well as horizontal flipping during training [36]. Evaluated on Market-1501 dataset this model achieves 85.2 rank-1, which is far beyond the current state-of-the-art performance [36,21,44,11,56,58,76]. For tracking, we define the appearance distance between two detections  $i$  and  $j$  as the cosine distance between their appearance embeddings  $d_a(i, j) = 1 - \frac{f_i \cdot f_j}{\|f_i\| \|f_j\|}$ . Moreover, the intersection over union (IoU) measure between two bounding boxes is given by as  $d_m(i, j) = IoU(p_i, p_j) = \frac{|p_i \cap p_j|}{|p_i \cup p_j|}$ .

#### 4.2 Datasets

We evaluate our approach on the MOTChallenge benchmark [16], in particular, on the MOT17 [38] and MOT20 [17] datasets. MOT17 contains 7 train and 7 test sequences of moving and static cameras. MOT20 varies from MOT17 by having 4 train and test sequences being heavily crowded with over 100 pedestrians in the scene. Both datasets offer public detection sets, where MOT17 provides three different detectors, while MOT20 provides one set of detections. However, they can also be evaluated on private detections. As common practice, for public detections we utilize bounding boxes refined by CenterTrack [80,49,24] as well as Tracktor [4,65,67,42,32,49,26] for MOT17 and by Tracktor for MOT20 [4,49,8]. In the private detection setting we utilize detections generated by YOLOX-X [18] with confidence values larger than a 0.5. We refer the reader to the supplementary material for training details. For our ablation studies, we utilize the commonly used split of the MOT17 train set into train and evaluation set where the first half of each sequence is used as train set and the second half of each sequence is used as evaluation set [80,63]. The benchmarks provide several evaluation metrics among which HOTA metric [35], IDF1 score [47] and MOTA [25] are the most common. While MOTA metric mainly is determined by object coverage and IDF1 mostly focus on identity preservation, HOTA balances both.

#### 4.3 Appearance Ablation

In this section, we investigate the impact of the design choices of our appearance model on the tracking performance. To this end, we do not utilize motion. In



diff $\tau$	IP	DA	FT	IDF1 $\uparrow$	HOTA $\uparrow$	MOTA $\uparrow$	IDSW $\downarrow$	FP $\downarrow$	FN $\downarrow$	MTR $\uparrow$	MLR $\downarrow$
				69.6	60.5	69.5	266	1130	15102	54.7	17.1
$\checkmark$				71.2	61.3	69.5	236	1131	15099	43.7	17.1
$\checkmark$	$\checkmark$			73.8	62.9	69.7	145	1129	15098	43.7	17.1
$\checkmark$	$\checkmark$	$\checkmark$		75.4	63.2	69.7	172	1124	15101	43.4	17.4
$\checkmark$	$\checkmark$		$\checkmark$	74.3	63.0	69.6	213	1079	15087	44.1	15.6

Table 1: Ablation of the single parts of our method on the validation set of CenterTrack pre-processed bounding boxes. IP=inactive proxies, DA=domain adaptation.

Table 1, we report our results on public detection bounding boxes. In the first row of Table 1, we show the performance of a basic appearance model. It uses ResNet50 [20] trained on Market-1501 dataset [78], the same network as used for our appearance model. We then ablate the model by adding our contributions: (i) different thresholds for active and inactive tracks (diff  $\tau$ ), (ii) the usage of the proxy distance for inactive tracks (IP), and (iii) on-the-fly domain adaptation, *i.e.*, target domain statistics for the batch-norm layers (DA). As shown, every module significantly improves the results in both IDF1 and HOTA scores.

**Different Handling of Active and Inactive Tracks.** As introduced in subsection 3.2, the distance histograms for active and inactive tracks differ significantly with respect to their means and variances. Therefore, this calls for different matching thresholds  $\tau_i$ . In the second row in Table 1, we show that utilizing different thresholds for active and inactive tracks (diff  $\tau$ ) improves our tracking performance by 1.6 percentage points (pp) in IDF1 and 0.8pp in HOTA. Moreover, utilizing our proxy distance (IP) computation instead of the last detection for inactive tracks adds further 2.6pp in IDF1 and 1.6pp in HOTA.

**On-the-fly domain adaptation.** Additionally, we leverage our on-the-fly domain adaptation (DA) introduced in Subsection 3.2 that accounts for differences among the sequences, allowing use to utilize more unified thresholds. By using it, we gain another 1.6pp in IDF1 and 0.3pp in HOTA metrics. One could argue that fine-tuning the model on MOT17 train sequences would have the same effect as our proposed domain adaptation. We try this and show results in the last row. For this evaluation, we split the 7 train sequences into 3 cross validation splits and fine-tune one model for each split. This is necessary as the same identities are given if a sequence is split along the temporal domain. Despite fine-tuning also significantly improves the performance it does not surpass our model with DA. We argue that the model is fine-tuned on tracking sequences, but the sequences still differ in their distributions among each other.

#### 4.4 Analysing the Strengths of Motion and Appearance

In this subsection, we analyze the performance of our appearance cues as introduced in Subsection 3.2 to find their strengths with respect to given tracking conditions, namely, visibility level of the detection, occlusion time of the track, and camera movement. We also analyze the complementary performance of a

linear motion model that we introduce in the following. For the analysis in this subsection and the ablation experiments in Subsection 4.5, we apply our approach on several private trackers. We note that this is not a state-of-the-art comparison, as we do not operate on plain detections, and emphasize that those experiments are solely used for analysis and to show the potential of our appearance and motion cues to improve current trackers.

**Linear Motion Model.** While many works apply more complex, motion models, *e.g.*, Kalman Filters [75,61], social motion models [29], or utilize detectors as motion model [4,80], we purposely choose a simple linear model for our experiments. Although the world does not move with constant velocity, many short term movements, as in the case for two consecutive frames, can be approximated with linear models and assuming constant velocity. Given detections of a track  $j$ , we compute the mean velocity  $v_j$  between consecutive detections and predict the current position of a track by

$$\hat{p}_j^t = \hat{p}_j^{t-1} + v_j \cdot \Delta t, \quad (3)$$

where  $\hat{p}_j^{t-1}$  is the position of the previous detection,  $p_{j^{t-1}}$  for active tracks and the predicted position  $\hat{p}_j^{t-1}$  of time step  $t-1$  for inactive tracks.  $\Delta t$  is the time difference from one frame to another. To obtain the motion distance between the new detections and the tracks, we compute IoU between the position of a new detection  $p_i$  and  $\hat{p}_j^t$ . We also visualize the corresponding distance histogram in Fig 3(c), showing that distance histograms between detections and tracks of the same and different identities are well separated for active tracks. In the following, we underline this observation by showing that this simple motion model is able to solve most situations.

**Analysis Setup and Intuition.** For our analysis, we investigate on the rate of correct associations ( $RCA$ ) on MOT17 validation set [16], which we define as:

$$RCA = \frac{TP-Ass}{FP-Ass + TP-Ass}, \quad (4)$$

where TP-Ass and FP-Ass represents true positive and false positive association, respectively. We average RCA over the sets of pre-processed private detections from several trackers (see Section 4.5) to get less noisy statistics.

Intuitively, motion should perform well for short-term associations as pedestrians only undergo small displacements, while appearance should be able to

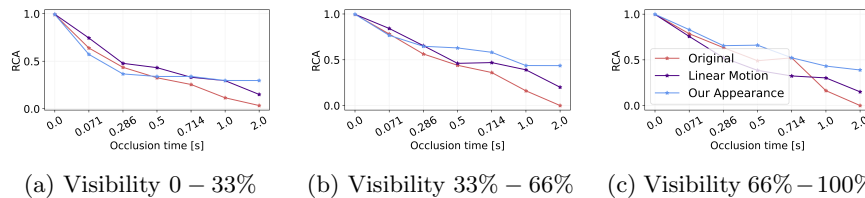


Fig. 5: RCA with respect to different visibility levels for short-term vs. long-term associations.

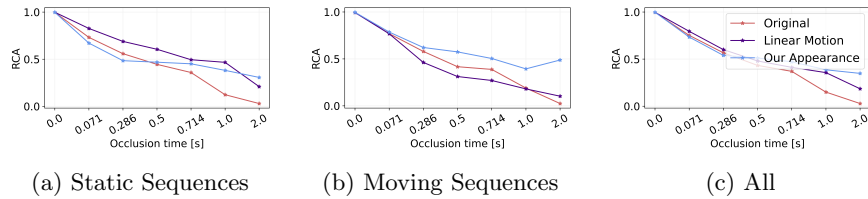


Fig. 6: RCA for static, moving, and all sequences with respect to short-term vs. long-term associations.

correctly do long-term associations. At the same time, motion should struggle to model long-term pedestrian behaviour, while appearance should be less robust with respect to occlusions as they highly influence appearance features.

**Observations.** We visualize RCA between detections and trajectories with increasing occlusion time for different visibility levels (see Figure 5). For example, in Figure 5(a) we plot RCA for reappearing bounding boxes that are 0 – 33% visible. We observe that for highly visible bounding boxes appearance performs better with respect to long-term as well as short-term occlusions. On the other hand, the lower the visibility, the higher the tendency of motion performing better with respect to long-term occlusions. This raises the following question: Why does motion not perform as good as appearance for short-term associations on highly visible bounding boxes? The motion of non-occluded pedestrians should not exhibit highly non-linear motion. Moreover, it is questionable why motion is able to perform long-term associations correctly. Therefore, we analyze the performance of motion and appearance for static and moving sequences with respect to short-term vs. long-term associations as well as visibility (see Figure 10 and Figure 9). We observe that motion is a strong cue in low visibility, *i.e.*, occluded scenarios, however struggles in moving sequences. Especially for static sequences, the linear motion model performs better with respect to long-term associations than appearance. We show a more detailed analysis in supplementary.

**Conclusion.** In conclusion the interplay of three factors mainly influence the performance of motion and appearance: visibility, occlusion time, and camera motion. However, we saw that appearance and motion complement each other well with respect to those factors. Hence, we now move on towards creating a strong trackers that combines our appearance and a simple linear motion model.

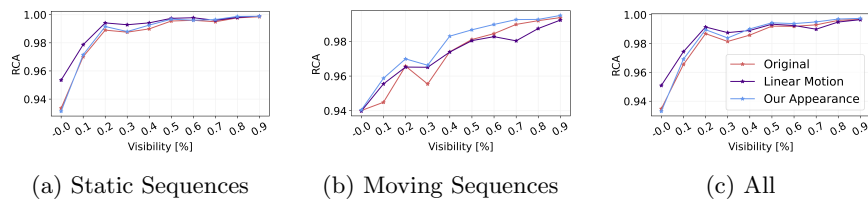


Fig. 7: RCA for static, moving, and all sequences with respect to different visibility levels.

#### 4.5 Simple cues lead to a strong tracker

In this subsection, we ablate the combination of appearance and motion into a simple Hungarian-based online tracker. We use the same setting as in Subsection 4.4, *i.e.*, we apply our approach upon other trackers. Hence, we only report metrics related to the association performance, *i.e.*, IDF1, and HOTA in Subsection 4.5, as our goal is not to improve on the MOTA metric, which is heavily dependent on detection performance. We visualize the results in Figure 8, where markers and colors define which motion and appearance model is used, respectively. The blue bars represent the average occlusion level of detection bounding boxes of the different trackers.

**Appearance.** Compared to the performance of the original trackers, our appearance model improves the performance significantly for detection sets with lower average occlusion level (Figure 8). In detection sets with high occlusion, pure appearance struggles, confirming that it is not suited for associations in those scenarios.

**Motion.** Interestingly, applying only the simple linear motion model without appearance always improves or performs on par with the original trackers. Utilizing a Kalman filter instead of the linear motion model, performs slightly worse in four (three) out of seven trackers, slightly better in one (two), and on par in one (one) in IDF1 (HOTA). This further highlights the strength of the simple linear motion model.

**Combination.** We also visualize the performance of our model, *i.e.*, our appearance combined with linear motion model. For all combinations we choose a simple sum. Moreover, we visualize the performance of our appearance model with Kalman filter. Figure 8 shows that using a Kalman filter instead of the linear motion model does not impact the performance notably. However, our combination improves the performance significantly compared to when using the motion models or our appearance alone.

We now show how our simple online Hungarian-based tracker, using strong appearance cues and a simple linear motion model, reaches a new state-of-the-art on two datasets, using both public and private detections.

#### 4.6 Public Detections

**MOT17.** We now compare our method with several state-of-the-art methods [69,9,42,68,64,4,65,32,67,2,80,49,26] in public detections. As we show in Table 2, our model improves over the best previous method TrackPool-T [26] by 3.8*pp* in IDF1 and ArTIST-C [49] 2.0*pp* in HOTA. As expected, we do not improve much on the MOTA metric, as it is mostly dependent on the detection performance, and we do not add new detection bounding boxes.

**MOT20.** We compare to state-of-the-art approaches on the public setting of MOT20 [5,33,1,4,49]. Despite the complexity of the sequences being heavily crowded and exhibiting difficult lightning conditions, our model improves the state-of-the-art [4] by 2.3*pp* in IDF1 and 1.3*pp* in HOTA metric (see Table 2). This shows that the combination of our strong appearance cues and the linear

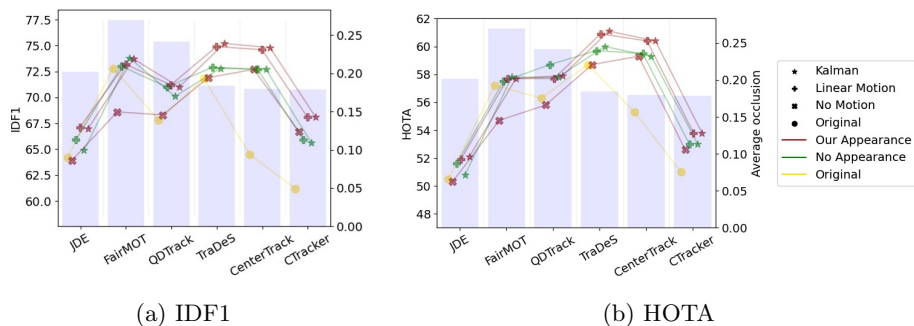


Fig. 8: Analysis of the contribution of Appearance and motion cues as well as their combination upon JDE [61], FairMOT [75], QDTrack [40], TraDeS [63], CenterTrack [80], CTracker [41]

motion automatically adapts to the underlying conditions of higher occlusion levels. Recall, we never train our appearance model on any of these sequences.

#### 4.7 Private Detections

**MOT17.** In the private detection setting, we first compare to MOT17 state-of-the-art approaches [55,41,39,63,80,40,75,59,53,60]. As shown in Table 2, we improve the current state-of-the-art CorrTracker [59] by 1.6*pp* in IDF1, and by 1.2*pp* over CorrTracker [59] and CrowdTracker [53] in HOTA.

**MOT20.** In the private detection setting in MOT20, we compare to [74,75,53,60] and improve over the previous state-of-the-art approach CrowdTracker [53] by 5.4*pp* in IDF1 and 4.4*pp* HOTA metric. Our approach is able to fully leverage the additional available bounding boxes in the private detection setting compared to the public detection setting, substantially increasing identity preservation in all experiments.

## 5 Conclusion

In this paper we revisit the TbD paradigm by our simple yet strong tracker. We introduce a spiced-up appearance model that handles active and inactive trajectories differently. Moreover, it adapts itself to the test sequences by applying an on-the-fly domain adaptation. In our analysis we show, that our appearance model and a simple linear motion model complement each other with respect to visibility, occlusion time, and camera movement. By combining both cues our approach outperforms current state-of-the-art trackers on MOT17 and MOT20 datasets. In public detection setting we improve by up to 3.86*pp* in IDF1 and 2.0*pp* in HOTA metric while in the private setting by up to 5.4*pp* in IDF1 and 4.4*pp* in HOTA.

	HOTA $\uparrow$	IDF1 $\uparrow$	MOTA $\uparrow$	IDSW $\downarrow$	AssA $\uparrow$	MTR $\uparrow$	MLR $\downarrow$
<i>Public MOT17</i>							
FAMNet [13]	-	48.7	52.0	3072	-	19.1	<b>33.4</b>
OneShotDA [68]	36.9	54.0	51.4	2188	43.5	21.2	37.3
MOTDT [9]	41.2	52.7	50.9	2474	41.4	17.5	35.7
TAMA [69]	42.0	53.5	50.3	2192	43.3	19.2	37.5
DeepMOT <sup>†</sup> [65]	42.4	53.8	53.7	1947	42.7	19.4	36.6
UMA [67]	-	54.4	53.1	2251	-	21.5	31.8
STRN [64]	42.6	56.0	50.9	2397	44.2	18.9	33.8
Tracktor v2 <sup>†</sup> [4]	44.8	55.1	56.3	1987	45.1	21.1	35.3
GNNMatch <sup>‡</sup> [14]	45.4	56.3	57.3	1911	45.2	24.4	33.4
GSM <sup>†</sup> [32]	45.7	57.8	56.4	<b>1485</b>	47.0	22.2	34.5
UNS <sup>†</sup> [2]	46.4	58.3	56.8	1911	<b>47.9</b>	22.8	37.4
UnsupTrack <sup>‡</sup> [24]	46.9	58.1	<b>61.7</b>	1864	45.2	27.2	32.4
TrackPool <sup>†</sup> [26]	-	<b>60.5</b>	55.9	<b>1188</b>	-	20.5	36.7
CenterTrack <sup>‡</sup> [80]	<b>48.2</b>	59.6	<b>61.5</b>	3039	47.8	<b>34.6</b>	<b>24.6</b>
ArTIST-C <sup>‡</sup> [49]	<b>48.9</b>	<b>59.7</b>	<b>62.3</b>	2062	<b>48.3</b>	<b>29.1</b>	34.0
Ours <sup>†</sup>	47.0	59.6	56.4	1517	49.5	21.1	35.6
Ours <sup>‡</sup>	<b>50.9</b>	<b>64.2</b>	<b>61.7</b>	<b>1639</b>	<b>52.8</b>	<b>26.3</b>	<b>32.2</b>
<i>Private MOT17</i>							
DAN [55]	39.3	49.5	52.4	8431	36.2	21.4	30.7
TubeTK [39]	48.0	58.6	63.0	5727	45.1	31.2	19.9
CTracker [41]	49.0	57.4	66.6	5529	45.2	32.2	24.2
CenterTrack [80]	52.2	64.7	67.8	<b>3039</b>	51.0	34.6	18.5
TraDeS [63]	52.7	63.9	69.1	3555	50.8	37.3	20
QDTrack [40]	53.9	66.3	68.7	3378	52.7	<b>49.0</b>	16.8
GSDT [60]	55.2	66.5	73.2	3891	51.0	41.7	17.5
FairMOT [75]	<b>59.3</b>	<b>72.3</b>	73.7	3303	58.0	43.2	17.3
CrowdTrack [53]	60.3	<b>73.6</b>	<b>75.6</b>	<b>2544</b>	<b>59.3</b>	46.5	<b>12.2</b>
CorrTracker [59]	<b>60.7</b>	<b>73.6</b>	<b>76.5</b>	3369	<b>58.9</b>	<b>47.6</b>	<b>12.7</b>
Ours	<b>61.9</b>	<b>75.2</b>	<b>78.7</b>	<b>2007</b>	<b>60.5</b>	<b>49.2</b>	<b>14.4</b>
<i>Public MOT20</i>							
TFT [33]	33.0	35.6	45.1	6492	26.3	<b>32.9</b>	<b>18.9</b>
GMPHD [1]	35.6	43.5	44.7	7492	32.0	23.6	<b>22.1</b>
SORT [5]	36.1	45.1	42.7	4470	35.9	16.7	<b>26.2</b>
ArTIST <sup>†</sup> [49]	<b>41.6</b>	<b>51.0</b>	<b>53.6</b>	<b>1531</b>	<b>40.2</b>	<b>31.6</b>	28.1
Tracktor v2 <sup>†</sup> [4]	<b>42.1</b>	<b>52.7</b>	<b>52.6</b>	<b>1648</b>	<b>42.0</b>	<b>29.4</b>	26.7
Ours <sup>†</sup>	<b>43.4</b>	<b>55.0</b>	<b>52.7</b>	<b>1437</b>	<b>44.7</b>	29.1	26.8
<i>Private MOT20</i>							
MLT [74]	43.2	54.6	48.9	<b>2187</b>	44.1	30.9	22.1
GSDT [60]	53.6	<b>67.5</b>	<b>67.1</b>	3230	<b>52.7</b>	53.1	<b>13.2</b>
FairMOT [75]	<b>54.6</b>	67.3	61.8	5243	54.7	<b>68.8</b>	<b>7.5</b>
CrowdTrack [53]	<b>55.0</b>	<b>68.2</b>	<b>70.7</b>	3198	<b>52.6</b>	<b>54.9</b>	<b>12.1</b>
Ours	<b>59.4</b>	<b>73.6</b>	<b>71.3</b>	<b>1219</b>	<b>60.3</b>	<b>56.3</b>	15.8

Table 2: Comparison to state-of-the-art public and private detection trackers on both MOT17 and MOT20. **Bold** represents the best results, **red** the second best, and **blue** the third best. <sup>†</sup> and <sup>‡</sup> indicate bounding boxes refined by Tracktor [4] and CenterTrack [80], respectively.

## A Supplementary Material

### A.1 Computation of Rate of Correct Associations

Given the output file of a tracker, to compute the rate of correct associations (RCA), we first match the given detections to ground truth identities (of MOT17 training set) following the same matching as the one used for the computation of the MOTA metric [25]. For each detection  $o_i$ , we then find the last detection that was assigned to the same ground truth identity  $o_{i,prev}$ . If  $o_i$  was assigned to the same tracker identity as  $o_{i,prev}$ , we count it as true positive association (TP-Ass), and if it was assigned to a different tracker identity, we count it as a false positive association (FP-Ass).

To get the performance for different amounts of visibility and occlusion time, we assign  $o_i$  to different bins. For example, when we investigate the performance for visibility 0–33%, we take only into account the detections  $o_i$  that are 0–33% visible. Same holds for occlusion: if we investigate occlusion time 0.5–0.7s, we only take detections  $o_i$  into account whose prior detection of the same ground truth identity was 0.5–0.7s ago.

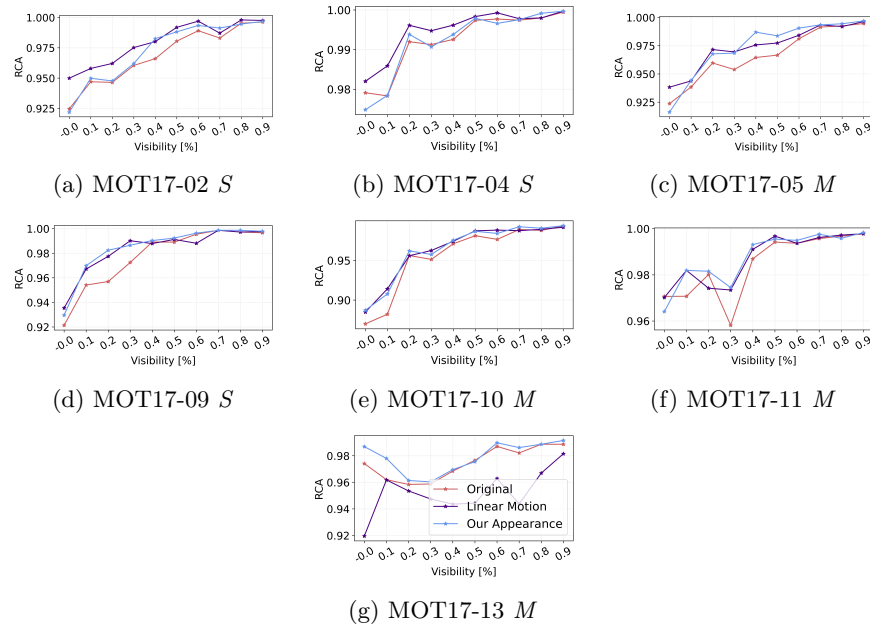
This procedure allows us to investigate the performance of different trackers with respect to different influencing factors solely based on the detection output files.

### A.2 A detailed analysis of Rate of Correct Associations per sequence

We show a per sequence analysis of the rate of correct associations (RCA) of motion and appearance with respect to visibility in Figure 9, and short-term vs. long-term association in Figure 10.  $M$  indicates moving sequence and  $S$  indicates static sequence.

With respect to visibility (see Figure 9), motion cues perform better especially in the static sequences MOT17-02 and MOT17-04. In the static sequence MOT17-09, which is recorded from a low viewpoint, and the moving sequences MOT17-05, MOT17-10, and MOT17-11, motion and appearance perform approximately on par. In MOT17-13, which shows heavy camera movements, the performance of the motion model drops significantly. Those observations show that for suitable camera angles in static sequences, motion outperforms appearance cues, while for sequences with severe camera movement, appearance outperforms motion.

Investigating different occlusion times (see Figure 9) shows that all moving sequences show a higher RCA for appearance compared to motion cues. For static sequences, motion performs slightly better in MOT17-02 and MOT17-04. In the static sequence MOT17-09, the sequence recorded from a low viewpoint, both perform approximately on par. This shows that for suitable camera angles, motion is a good cue for long-term associations in static cameras, while appearance is needed in moving sequences.

Fig. 9: RCA for static *S* and moving *M* sequences with respect to visibility.

### A.3 Intersection point computation

In Section 3.2 of the main paper, we show that the intersection points of the histograms when using our on-the-fly domain adaptation vary less compared to when not using it. We use the histograms to visualize and approximate the real underlying distance distribution, *i.e.*, probability density functions (PDF). The intersection point of two functions  $f_1(x)$  and  $f_2(x)$  is given when  $f_1(x) = f_2(x)$ . As we only have the approximation of the underlying PDFs, we also have to approximate the intersection point. The histogram  $h_i = \{b, n_i, \}$  is defined by the bins  $b \in \mathbf{R}^{N_b}$  dividing the  $x$ -axis into equidistant bins and the corresponding bin counts  $n_i \in \mathbf{R}^{N_b}$ .  $N_b$  is the number of bins and the elements in  $b$  represent the lower bound of the bins. Note that we assume the same underlying bins for all histograms  $h_i$ .

To approximate the intersection point of two histograms, we first compute the absolute distance between both in all bins:

$$d_{1,2} = |n_1 - n_2| \quad (5)$$

The intersection point of the two histograms is given at the  $k^*$ -th bin  $b^{k^*}$  where we have  $d_{1,2}^{k^*} \approx 0$ . Therefore, we find the intersection point by:

$$k^* = \arg \min_k d_{1,2}^k \quad (6)$$

However,  $d_{1,2}^k \approx 0$  may also hold for the bounds of the histograms, as in those regions  $n_1 \approx 0$  and  $n_2 \approx 0$  might hold. Hence, we restrict the intersection point



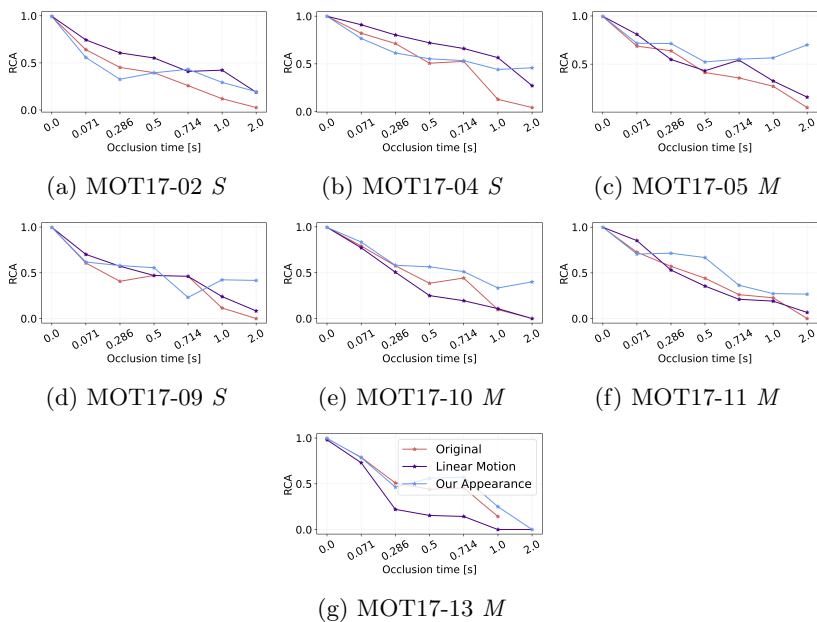


Fig. 10: RCA for static  $S$  and moving  $M$  sequences with respect to short-term vs. long-term associations.

where  $d_{1,2}^k \approx 0$  to lie between the maxima of the histograms. The maximal count  $n_i^{m_i^*}$  of a histogram  $h_i$  is given at  $m_i^*$ -th bin  $b^{m_i^*}$  where  $m_i^*$  is defined by:

$$m_i^* = \arg \max_m n_i^m \quad (7)$$

Assume that  $b^{m_1^*} \leq b^{m_2^*}$ . The intersection point is finally given by:

$$k^* = \arg \min_k d_{1,2}^k \\ \text{subject to } b^{m_1^*} \leq b^k \leq b^{m_2^*}$$

#### A.4 Different Proxies

We now explore different proxies for the distance computation between new detections and inactive tracks. To this end, we generate feature vectors with our CNN, *i.e.*, ResNet50 with additional downsampling layer at the end and we normalize them before further processing. As introduced in the main paper, we utilize the mean of the distances of a new detection to all detections of an inactive track. The cosine distance between new detection  $i$  and inactive track  $k$  is then given by:

$$\tilde{d}(i, k) = \frac{1}{N_k} \sum_{n=1}^{N_k} d(f_i, f_k^n) = \frac{1}{N_k} \sum_{n=1}^{N_k} 1 - \frac{f_i \cdot f_k^n}{\|f_i\| \cdot \|f_k^n\|} = 1 - \frac{1}{N_k} \sum_{n=1}^{N_k} f_i \cdot f_k^n \quad (8)$$

where  $N_k$  is the number of detections in the inactive track and  $f_k^n$  is the feature vector corresponding to its  $n$ -th detection. We omit  $\|f_i\| \cdot \|f_k^n\|$  as we normalize all feature vectors.

Another option is to first compute a proxy feature vector and then compute the distance between a new detection and the proxy feature vector. We investigate four proxy feature vector computations and report results on the validation set of CenterTrack-refined public detections.

**Mean Feature Vector.** The mean feature vector of all detections in the inactive track  $k$  which is also used in Tracktor [4] is given by

$$\tilde{f}_k = \frac{1}{N_k} \sum_{n=0}^{N_k} f_k^n \quad (9)$$

Computing the cosine distance of this mean feature vector leads to

$$\tilde{d}(i, k) = 1 - \frac{f_i \cdot \frac{1}{N_k} \sum_{n=1}^{N_k} f_k^n}{\|f_i\| \cdot \|\frac{1}{N_k} \sum_{n=1}^{N_k} f_k^n\|} = 1 - \frac{\sum_{n=1}^{N_k} f_i \cdot f_k^n}{\|\sum_{n=1}^{N_k} f_k^n\|} \quad (10)$$

This means it differs from the proxy distance by the normalization constant  $\frac{1}{\|\sum_{n=1}^{N_k} f_k^n\|}$ .

**Mode Feature Vector.** Compared to the mean feature vector, the feature vector of inactive track  $k$  is given by the value that appeared most in each feature dimension.

**Median Feature Vector.** Viewing  $f_k^n$  as a random variable, in each dimension the median feature vector contains the value for which 50% of the probability mass of feature values in this dimension lies on the right and left of it, *i.e.*, it divides the probability mass into two equal masses.

**Exponential Moving Average Feature Vector.** Utilizing the exponential moving average (EMA) as feature vector as done in JDE [46] or FairMOT [75] means that at given a new detection, the feature vector is updated by:

$$\tilde{f}_k^t = \tilde{f}_k^{t-1} * \alpha + f_k^t * (1 - \alpha) \quad (11)$$

where  $\tilde{f}_k^{t-1}$  is the EMA feature vector at the previous time step,  $f_k^t$  is the feature vector of the new detection, and  $\alpha = 0.9$  is a weighting factor. The EMA feature vectors build on the underlying assumption that feature vectors should change only slightly and, therefore, smooths the feature vector development.

We show the performance of the different approaches in Table 3. Although the performance of the mean feature vectors alone is competitive with our proxy distance, in combination with the linear motion model, the IDF1 and HOTA metric drop significantly by 4.9pp and 1.9pp, respectively. The opposite holds for moving average feature vectors, where the IDF1 and HOTA metric drop significantly when using them alone, by 5.6pp and 2.8pp, respectively, and only by 0.9pp and 0.5pp when combined with the Linear motion model. While mode feature vectors alone perform slightly worse than our proxy distance when applied alone, they nearly perform on par when applied together with the linear motion

	Appearance			Appearance + Linear Motion		
	HOTA $\uparrow$	IDF1 $\uparrow$	MOTA $\uparrow$	HOTA $\uparrow$	IDF1 $\uparrow$	MOTA $\uparrow$
Our Proxy	63.1	74.4	69.7	63.6	75.6	69.7
Mean Features	-0.2	-0.3	0.1	-1.9	-4.9	-0.1
Mode Features	-0.5	-0.4	0	-0.1	-0.1	0
Median Features	-1.3	-3.4	-0.1	-0.7	-1.5	0.1
Moving Average Features	-2.8	-5.6	-0.3	-0.5	-0.9	0

Table 3: Comparison of different proxy generation methods.

model. Finally, median feature vectors lead to a significant drop when applied alone by  $3.4pp$  and  $1.3pp$  in IDF1 and HOTA, but reduce their drop by half when combined with the linear motion model to  $1.5pp$  and  $0.7pp$ .

Overall, the experiments show that even when appearance performs well when applied alone, it does not imply that it also will perform well when combined together with motion using our combination scheme, emphasizing even more our appearance design choices.

## A.5 Memory

Compared to other approaches [4,52,75,46,32] that only keep inactive tracks for a fixed number of frames, called inactive patience, we keep all inactive tracks over the whole sequence. Hence, we are theoretically able to recover the identity after an occlusion of arbitrary length. To show that this choice does not lead to false matches during the association process, we visualize HOTA, IDF1, and MOTA for different inactive patience values in Figure 11, Figure 12, and Figure 13, respectively. We use the same setting as in Subsections 4.4 and 4.5 in the main paper. The performance drops heavily for inactive patience 0 and then only slightly changes up to using all frames of a sequence.

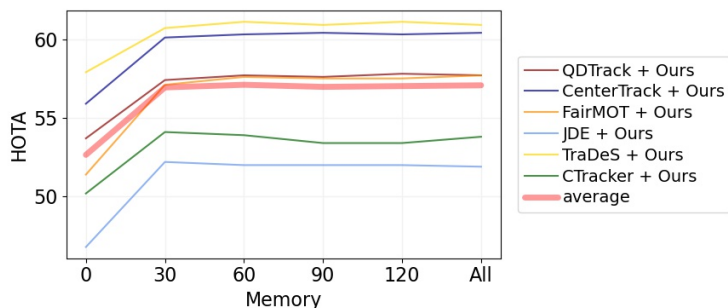


Fig. 11: HOTA performance with respect to different memory patience values.

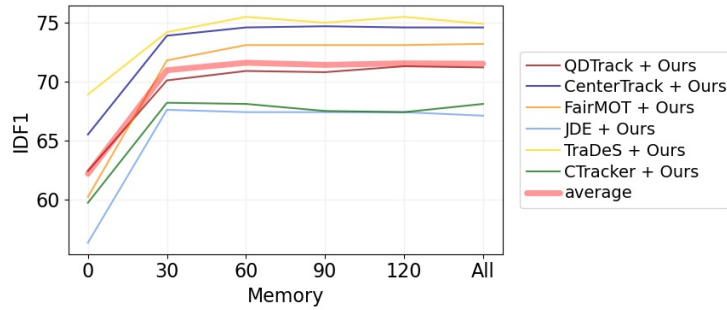


Fig. 12: IDF1 performance with respect to different memory patience values.

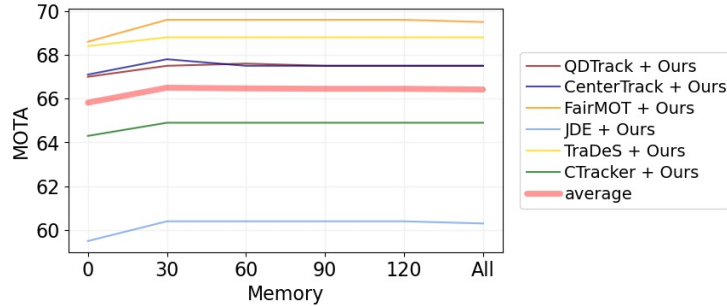


Fig. 13: MOTA performance with respect to different memory patience values.

## A.6 Training Details

In this section, we give the training details of the detector used to generate our private detection bounding boxes. The weights of the detector we utilize were initialized by COCO-pretrained [30] weights, and trained for another 80 epochs jointly on MOT17, ETHZ, CrowdHuman, and CityPerson. Input images are resized too  $1440 \times 800$  and Mosaic [7] and MixUp [72] data augmentation techniques are applied. During training, a batchsize of 48 as well as SGD with weight decay of  $5 \times 10^{-4}$  and momentum of 0.9 are utilized. As initial learning rate  $10^{-3}$  is used with 1 epoch warm-up and cosine annealing schedule.

## A.7 Adapting the Matching Thresholds $\tau_i$

As we introduced in the main paper, we use thresholds  $\tau_i$  to restrict the matchings to detection-track pairs of sufficient similarity. We find the thresholds by computing the mean  $\mu$  and standard deviation  $\sigma$  of the distances from new detections to active (*act*) and inactive (*inact*) tracks of the same (*s*) and different (*d*) identities. With this, we account for the distributions of the distances as visualized in the histograms. To be specific, we compute:

$$\tau_{act} = \mu_d^{act} - \sigma_s^{inact} \quad (12)$$



Fig. 14: Occlusion time: 2s, visibility of re-appearing pedestrian: 0.6.

$$\tau_{inact} = \mu_s^{inact} - 0.5 \cdot \sigma_s^{inact} \quad (13)$$

The former accounts for the fact that the histograms of distances to the same and different identities are well separated for active tracks, therefore, we can choose a looser threshold with respect to the distribution of distances to detections of different identities (see Figure 3 in the main paper). For inactive tracks, we chose the threshold to be lower than  $\mu_s^{inact}$ , as the distributions corresponding to the inactive tracks show significant overlap (see Figure 3 in the main paper).

Note, that for the ablations we do not use the same matching thresholds for the different settings, since the distance histograms significantly change between settings. This is, on the one hand, caused by the design choices of the distance matrix, as explained in Subsection 4.2 of the main paper. On the other hand, different detectors show different amounts of false positive and false negative detections. For example, a detector with more false negative examples and less false positives, might detect only well visible, high confidence bounding boxes which leads to better separated histograms of same and different identities.

## A.8 Visualizations

In this section, we visualize associations on CenterTrack re-fined public bounding boxes that our model is able to correctly associate while CenterTrack is not. Correct and wrong associations are determined in the same way as done for the computation of the RCA Section A.1. This means we determine wrong associations by first matching all detection bounding boxes to the ground truth IDs. A wrong association is given if the prior detection of the same ground truth ID as a current detection was assigned to a different tracker ID than the current detection. In the Figures 6-16, we visualize the prior detection on the left side and the current detection on the right side. All examples were associated wrongly by CenterTrack and correct by our approach. We give the time distance between the prior and the current frame in the caption as well as the visibility level of the re-appearing pedestrian. By our combination of appearance and motion, we are able to correctly associate pedestrians after long occlusions and low visibility in highly varying sequences.



Fig. 15: Occlusion time: 1.7s, visibility of re-appearing pedestrian: 0.3.

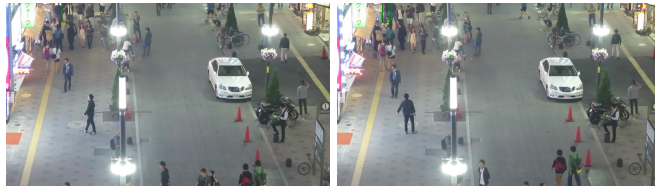


Fig. 16: Occlusion time: 1.1s, visibility of re-appearing pedestrian: 0.3.

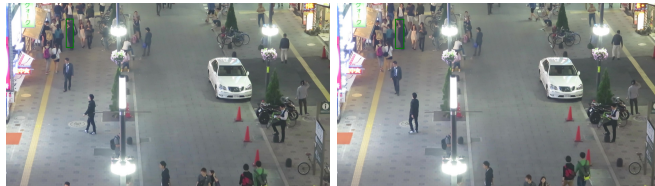


Fig. 17: Occlusion time: 0.6 s, visibility of re-appearing pedestrian: 0.3.

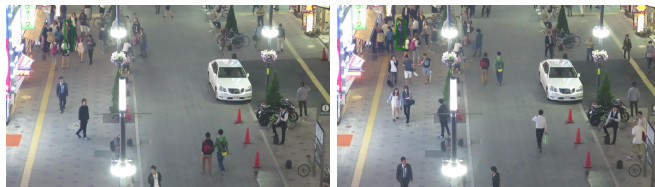


Fig. 18: Occlusion time: 9.4s, visibility of re-appearing pedestrian: 0.4.



Fig. 19: Occlusion time: 1.1s, visibility of re-appearing pedestrian: 0.5.



Fig. 20: Occlusion time: 1s, visibility of re-appearing pedestrian: 0.4.



Fig. 21: Occlusion time: 0.9s, visibility of re-appearing pedestrian: 0.2.



Fig. 22: Occlusion time: 1.1s, visibility of re-appearing pedestrian: 0.2.

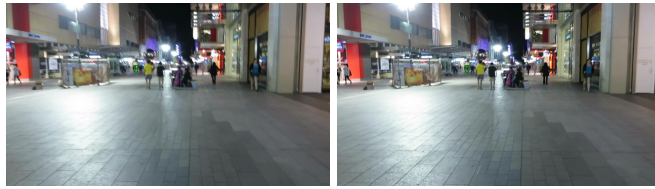


Fig. 23: Occlusion time: 0.1s, visibility of re-appearing pedestrian: 0.6.



Fig. 24: Occlusion time: 0.9s, visibility of re-appearing pedestrian: 0.5.



Fig. 25: Occlusion time: 0.2s, visibility of re-appearing pedestrian: 0.8.



## References

1. Baisa, N.L.: Occlusion-robust online multi-object visual tracking using a GM-PHD filter with cnn-based re-identification. *J. Vis. Commun. Image Represent.* **80**, 103279 (2021) [12](#), [14](#)
2. Bastani, F., He, S., Madden, S.: Self-supervised multi-object tracking with cross-input consistency. *NeurIPS* (2021) [12](#), [14](#)
3. Berclaz, J., Fleuret, F., Türetken, E., Fua, P.: Multiple object tracking using k-shortest paths optimization. *tPAMI* **33**(9), 1806–1819 (2011) [3](#)
4. Bergmann, P., Meinhardt, T., Leal-Taixé, L.: Tracking without bells and whistles. In: *ICCV* (2019) [1](#), [3](#), [5](#), [8](#), [10](#), [12](#), [14](#), [18](#), [19](#)
5. Bewley, A., Ge, Z., Ott, L., Ramos, F.T., Upcroft, B.: Simple online and realtime tracking. In: *ICIP* (2016) [3](#), [5](#), [12](#), [14](#)
6. Bochinski, E., Eiselein, V., Sikora, T.: High-speed tracking-by-detection without using image information. In: *AVSS* (2017) [3](#)
7. Bochkovskiy, A., Wang, C., Liao, H.M.: Yolov4: Optimal speed and accuracy of object detection. *arXiv abs/2004.10934* (2020) [20](#)
8. Brasó, G., Leal-Taixé, L.: Learning a neural solver for multiple object tracking. In: *CVPR* (2020) [3](#), [8](#)
9. Chen, L., Ai, H., Zhuang, Z., Shang, C.: Real-time multiple people tracking with deeply learned candidate selection and person re-identification. In: *ICME* (2018) [12](#), [14](#)
10. Chen, T., Ding, S., Xie, J., Yuan, Y., Chen, W., Yang, Y., Ren, Z., Wang, Z.: Abd-net: Attentive but diverse person re-identification. In: *ICCV* (2019) [2](#)
11. Cheng, D., Gong, Y., Zhou, S., Wang, J., Zheng, N.: Person re-identification by multi-channel parts-based CNN with improved triplet loss function. In: *CVPR* (2016) [1](#), [8](#)
12. Choi, S., Kim, T., Jeong, M., Park, H., Kim, C.: Meta batch-instance normalization for generalizable person re-identification. In: *CVPR* (2021) [4](#), [6](#)
13. Chu, P., Ling, H.: Famnet: Joint learning of feature, affinity and multi-dimensional assignment for online multiple object tracking. In: *ICCV* (2019) [14](#)
14. Dai, P., Weng, R., Choi, W., Zhang, C., He, Z., Ding, W.: Learning a proposal classifier for multiple object tracking. In: *CVPR* (2021) [8](#), [14](#)
15. Dai, Z., Chen, M., Gu, X., Zhu, S., Tan, P.: Batch dropblock network for person re-identification and beyond. In: *ICCV* (2019) [2](#)
16. Dendorfer, P., Osep, A., Milan, A., Schindler, K., Cremers, D., Reid, I., Roth, S., Leal-Taixé, L.: Motchallenge: A benchmark for single-camera multiple target tracking. *IJCV* **129**(4), 845–881 (2021) [8](#), [10](#)
17. Dendorfer, P., Rezatofighi, H., Milan, A., Shi, J., Cremers, D., Reid, I.D., Roth, S., Schindler, K., Leal-Taixé, L.: MOT20: A benchmark for multi object tracking in crowded scenes. *arXiv abs/2003.09003* (2020) [8](#)
18. Ge, Z., Liu, S., Wang, F., Li, Z., Sun, J.: YOLOX: exceeding YOLO series in 2021. *arXiv abs/2107.08430* (2021) [8](#)
19. Guo, S., Wang, J., Wang, X., Tao, D.: Online multiple object tracking with cross-task synergy. In: *CVPR* (2021) [3](#)
20. He, K., Zhang, X., Ren, S., Sun, J.: Deep residual learning for image recognition. In: *CVPR* (2016) [5](#), [8](#), [9](#)
21. Hermans, A., Beyer, L., Leibe, B.: In defense of the triplet loss for person re-identification. *arXiv abs/1703.07737* (2017) [1](#), [8](#)

22. Hornáková, A., Henschel, R., Rosenhahn, B., Swoboda, P.: Lifted disjoint paths with application in multiple object tracking. In: ICML (2020) [3](#)
23. Jiang, H., Fels, S.S., Little, J.J.: A linear programming approach for multiple object tracking. In: CVPR (2007) [3](#)
24. Karthik, S., Prabhu, A., Gandhi, V.: Simple unsupervised multi-object tracking. arXiv [abs/2006.02609](#) [8](#), [14](#)
25. Kasturi, R., Goldgof, D.B., Soundararajan, P., Manohar, V., Garofolo, J.S., Bowers, R., Boonstra, M., Korzhova, V.N., Zhang, J.: Framework for performance evaluation of face, text, and vehicle detection and tracking in video: Data, metrics, and protocol. tPAMI (2009) [8](#), [15](#)
26. Kim, C., Li, F., Alotaibi, M., Rehg, J.M.: Discriminative appearance modeling with multi-track pooling for real-time multi-object tracking. In: CVPR (2021) [3](#), [8](#), [12](#), [14](#)
27. Kuhn, H.W., Yaw, B.: The hungarian method for the assignment problem. Naval Res. Logist. Quart pp. 83–97 (1955) [1](#)
28. Leal-Taixé, L., Canton-Ferrer, C., Schindler, K.: Learning by tracking: Siamese CNN for robust target association. In: CVPR (2016) [3](#)
29. Leal-Taixé, L., Pons-Moll, G., Rosenhahn, B.: Everybody needs somebody: Modeling social and grouping behavior on a linear programming multiple people tracker. In: ICCV (2011) [3](#), [10](#)
30. Lin, T., Maire, M., Belongie, S.J., Hays, J., Perona, P., Ramanan, D., Dollár, P., Zitnick, C.L.: Microsoft COCO: common objects in context. In: ECCV (2014) [20](#)
31. Liu, L., Jiang, H., He, P., Chen, W., Liu, X., Gao, J., Han, J.: On the variance of the adaptive learning rate and beyond. In: ICLR (2020) [8](#)
32. Liu, Q., Chu, Q., Liu, B., Yu, N.: GSM: graph similarity model for multi-object tracking. In: IJCAI (2020) [5](#), [8](#), [12](#), [14](#), [19](#)
33. Lohn-Jaramillo, J., Jarrett, K., Ray, L.E., Granger, R., Bowen, E.F.W.: Time-first tracking: An efficient multiple-object tracking architecture for dynamic surveillance environments. In: ICPRAM (2021) [12](#), [14](#)
34. Lu, Z., Rathod, V., Votel, R., Huang, J.: Retinatrack: Online single stage joint detection and tracking. In: CVPR (2020) [3](#)
35. Luiten, J., Osep, A., Dendorfer, P., Torr, P.H.S., Geiger, A., Leal-Taixé, L., Leibe, B.: HOTA: A higher order metric for evaluating multi-object tracking. IJCV (2021) [8](#)
36. Luo, H., Gu, Y., Liao, X., Lai, S., Jiang, W.: Bag of tricks and a strong baseline for deep person re-identification. In: CVPR (2019) [1](#), [2](#), [8](#)
37. Meinhardt, T., Kirillov, A., Leal-Taixé, L., Feichtenhofer, C.: Trackformer: Multi-object tracking with transformers. arXiv [abs/2101.02702](#) (2021) [1](#), [3](#)
38. Milan, A., Leal-Taixé, L., Reid, I.D., Roth, S., Schindler, K.: MOT16: A benchmark for multi-object tracking. arXiv [abs/1603.00831](#) (2016) [8](#)
39. Pang, B., Li, Y., Zhang, Y., Li, M., Lu, C.: Tubetk: Adopting tubes to track multi-object in a one-step training model. In: CVPR (2020) [3](#), [13](#), [14](#)
40. Pang, J., Qiu, L., Li, X., Chen, H., Li, Q., Darrell, T., Yu, F.: Quasi-dense similarity learning for multiple object tracking. In: CVPR (2021) [3](#), [13](#), [14](#)
41. Peng, J., Wang, C., Wan, F., Wu, Y., Wang, Y., Tai, Y., Wang, C., Li, J., Huang, F., Fu, Y.: Chained-tracker: Chaining paired attentive regression results for end-to-end joint multiple-object detection and tracking. In: ECCV (2020) [1](#), [3](#), [13](#), [14](#)
42. Peng, J., Wang, T., Lin, W., Wang, J., See, J., Wen, S., Ding, E.: TPM: multiple object tracking with tracklet-plane matching. Pattern Recognition (2020) [8](#), [12](#)

43. Pirsiavash, H., Ramanan, D., Fowlkes, C.C.: Globally-optimal greedy algorithms for tracking a variable number of objects. In: CVPR (2011) [3](#)
44. Quan, R., Dong, X., Wu, Y., Zhu, L., Yang, Y.: Auto-reid: Searching for a part-aware convnet for person re-identification. In: ICCV (2019) [1](#), [8](#)
45. Redmon, J., Farhadi, A.: YOLO9000: better, faster, stronger. In: CVPR (2017) [3](#)
46. Ren, S., He, K., Girshick, R.B., Sun, J.: Faster R-CNN: towards real-time object detection with region proposal networks. In: NeurIPS (2015) [1](#), [3](#), [5](#), [18](#), [19](#)
47. Ristani, E., Solera, F., Zou, R.S., Cucchiara, R., Tomasi, C.: Performance measures and a data set for multi-target, multi-camera tracking. In: ECCV Workshops (2016) [8](#)
48. Sadeghian, A., Alahi, A., Savarese, S.: Tracking the untrackable: Learning to track multiple cues with long-term dependencies. In: ICCV (2017) [3](#)
49. Saleh, F.S., Aliakbarian, S., Rezaatofghi, H., Salzmann, M., Gould, S.: Probabilistic tracklet scoring and inpainting for multiple object tracking. In: CVPR (2021) [8](#), [12](#), [14](#)
50. Shao, S., Zhao, Z., Li, B., Xiao, T., Yu, G., Zhang, X., Sun, J.: Crowddhuman: A benchmark for detecting human in a crowd. arXiv [abs/1805.00123](#) (2018) [1](#)
51. Son, J., Baek, M., Cho, M., Han, B.: Multi-object tracking with quadruplet convolutional neural networks. In: CVPR (2017) [3](#)
52. Stadler, D., Beyerer, J.: Improving multiple pedestrian tracking by track management and occlusion handling. In: CVPR (2021) [1](#), [5](#), [19](#)
53. Stadler, D., Beyerer, J.: On the performance of crowd-specific detectors in multi-pedestrian tracking. In: AVSS (2021) [13](#), [14](#)
54. Sun, P., Jiang, Y., Zhang, R., Xie, E., Cao, J., Hu, X., Kong, T., Yuan, Z., Wang, C., Luo, P.: Transtrack: Multiple-object tracking with transformer. arXiv [abs/2012.15460](#) (2020) [1](#), [3](#)
55. Sun, S., Akhtar, N., Song, H., Mian, A., Shah, M.: Deep affinity network for multiple object tracking. tPAMI **43**(1), 104–119 (2021) [13](#), [14](#)
56. Sun, Y., Zheng, L., Yang, Y., Tian, Q., Wang, S.: Beyond part models: Person retrieval with refined part pooling (and A strong convolutional baseline). In: ECCV (2018) [1](#), [8](#)
57. Tokmakov, P., Li, J., Burgard, W., Gaidon, A.: Learning to track with object permanence. ICCV (2021) [3](#)
58. Varior, R.R., Haloi, M., Wang, G.: Gated siamese convolutional neural network architecture for human re-identification. In: ECCV (2016) [1](#), [8](#)
59. Wang, Q., Zheng, Y., Pan, P., Xu, Y.: Multiple object tracking with correlation learning. In: CVPR (2021) [13](#), [14](#)
60. Wang, Y., Kitani, K., Weng, X.: Joint object detection and multi-object tracking with graph neural networks. In: ICRA (2021) [13](#), [14](#)
61. Wang, Z., Zheng, L., Liu, Y., Li, Y., Wang, S.: In: ECCV (2020) [3](#), [5](#), [10](#), [13](#)
62. Wojke, N., Bewley, A., Paulus, D.: Simple online and realtime tracking with a deep association metric. In: ICIP (2017) [3](#)
63. Wu, J., Cao, J., Song, L., Wang, Y., Yang, M., Yuan, J.: Track to detect and segment: An online multi-object tracker. In: CVPR (2021) [1](#), [8](#), [13](#), [14](#)
64. Xu, J., Cao, Y., Zhang, Z., Hu, H.: Spatial-temporal relation networks for multi-object tracking. In: ICCV (2019) [12](#), [14](#)
65. Xu, Y., Osep, A., Ban, Y., Horaud, R., Leal-Taixé, L., Alameda-Pineda, X.: How to train your deep multi-object tracker. In: CVPR (2020) [1](#), [3](#), [8](#), [12](#), [14](#)
66. Yang, F., Choi, W., Lin, Y.: Exploit all the layers: Fast and accurate CNN object detector with scale dependent pooling and cascaded rejection classifiers. In: CVPR (2016) [3](#)

67. Yin, J., Wang, W., Meng, Q., Yang, R., Shen, J.: A unified object motion and affinity model for online multi-object tracking. In: CVPR (2020) [8](#), [12](#), [14](#)
68. Yoon, K., Gwak, J., Song, Y., Yoon, Y., Jeon, M.: Oneshotda: Online multi-object tracker with one-shot-learning-based data association. IEEE Access **8**, 38060–38072 (2020) [12](#), [14](#)
69. Yoon, Y., Kim, D.Y., Song, Y., Yoon, K., Jeon, M.: Online multiple pedestrians tracking using deep temporal appearance matching association. Inf. Sci. **561**, 326–351 (2021) [12](#), [14](#)
70. Yu, F., Li, W., Li, Q., Liu, Y., Shi, X., Yan, J.: POI: multiple object tracking with high performance detection and appearance feature. In: ECCV (2016) [3](#)
71. Zeng, F., Dong, B., Wang, T., Chen, C., Zhang, X., Wei, Y.: MOTR: end-to-end multiple-object tracking with transformer. arXiv [abs/2105.03247](#) (2021) [1](#), [3](#)
72. Zhang, H., Cissé, M., Dauphin, Y.N., Lopez-Paz, D.: Mixup: Beyond empirical risk minimization. In: ICLR (2018) [20](#)
73. Zhang, L., Li, Y., Nevatia, R.: Global data association for multi-object tracking using network flows. In: CVPR (2008) [3](#)
74. Zhang, Y., Sheng, H., Wu, Y., Wang, S., Ke, W., Xiong, Z.: Multiplex labeling graph for near-online tracking in crowded scenes. IEEE Internet Things J. **7**(9), 7892–7902 (2020) [13](#), [14](#)
75. Zhang, Y., Wang, C., Wang, X., Zeng, W., Liu, W.: Fairmot: On the fairness of detection and re-identification in multiple object tracking. IJCV **129**(11), 3069–3087 (2021) [1](#), [3](#), [5](#), [10](#), [13](#), [14](#), [18](#), [19](#)
76. Zhang, Z., Lan, C., Zeng, W., Chen, Z.: Densely semantically aligned person re-identification. In: CVPR (2019) [1](#), [8](#)
77. Zhao, Y., Zhong, Z., Yang, F., Luo, Z., Lin, Y., Li, S., Sebe, N.: Learning to generalize unseen domains via memory-based multi-source meta-learning for person re-identification. In: CVPR (2021) [4](#), [6](#)
78. Zheng, L., Shen, L., Tian, L., Wang, S., Wang, J., Tian, Q.: Scalable person re-identification: A benchmark. In: ICCV (2015) [2](#), [5](#), [8](#), [9](#)
79. Zhou, K., Xiang, T.: Torchreid: A library for deep learning person re-identification in pytorch. arXiv [arXiv:1910.10093](#) (2019) [2](#)
80. Zhou, X., Koltun, V., Krähenbühl, P.: Tracking objects as points. In: ECCV (2020) [1](#), [3](#), [8](#), [10](#), [12](#), [13](#), [14](#)
81. Zhuang, Z., Wei, L., Xie, L., Zhang, T., Zhang, H., Wu, H., Ai, H., Tian, Q.: Rethinking the distribution gap of person re-identification with camera-based batch normalization. In: ECCV (2020) [4](#), [6](#)